SANE: Safe Charging with Wave Interference

Yuan Yin*†, Dié Wu*†, Jing Gao*†, Jin Yang‡, Jilin Yang*†, Tang Liu*†
*College of Computer Science, Sichuan Normal University, Chengdu, Sichuan 610101, China
†Visual Computing and Virtual Reality Key Lab, Sichuan Normal University, Chengdu, Sichuan 610068, China
‡College of Computer Science, Sichuan University, Chengdu, Sichuan 610065, China
Email: {yuanyin, jinggao}@stu.sicnu.edu.cn, {wd, jilinyang, liutang}@sicnu.edu.cn, jinyang@scu.edu.cn

IEEE INFOCOM 2025 - IEEE Conference on Computer Communications | 979-8-3315-4305-1/25/$31.00 ©2025 IEEE | DOI: 10.1109/INFOCOM55648.2025.11044512

***Abstract*—With wireless power transfer becoming a popular technology for recharging devices in various fields, the accompanying potential threats of electromagnetic radiation (EMR) have attracted widespread attention from researchers. Although some state-of-the-art safe charging solutions have been developed to address EMR threats, they all ignore wave interference, resulting in a gap between their theoretical models and real-world applications. In this work, we focus on developing a safe charging scheme considering wave interference, termed Safe chArging with wave iNterferencE (SANE), aiming to maximize the overall charging utility while ensuring the EMR safety of critical locations. Specifically, we first build a charging model with wave interference to explore the impact of wave interference on the EMR intensity. Then, we devise a charger placement method that meets safe charging requirements while enabling devices to harvest maximum power from constructive interference. Finally, we conduct extensive simulations and field experiments to evaluate the effectiveness of SANE scheme. The results demonstrate that SANE not only ensures the EMR intensity at all critical locations remains below the safety threshold but also outperforms the comparison algorithms by an average of 89.65% in overall charging utility.**

***Index Terms*—electromagnetic radiation, wave interference, charger placement, wireless power transfer**

I. Introduction

Nowadays, Wireless Power Transfer (WPT) technology [1] has experienced rapid development due to its unique benefits, including contactless operation, no wiring, and easy maintenance. WPT enables power transmitters (*i.e.*, wireless chargers) to transfer energy to power receivers (*i.e.*, rechargeable devices) without any physical connection through electromagnetic waves. The Wireless Rechargeable Networks (WRNs) implemented with WPT technology have become a favorable alternative for prolonged network lifetime [2]–[11], alleviating the energy limitation problem in a variety of small battery-powered devices.

Despite the advantages offered by WRNs in various applications, such as healthcare [12]–[14], smart offices [15]–[17], and smart homes [18]–[20], the accompanying high electromagnetic radiation (EMR) has raised serious safety concerns for the human body exposed to it [21], [22]. For instance, when it comes to the WRNs deployed in smart offices, pregnant women working there may encounter severe health threats with long-term exposure to intense electromagnetic waves. Similarly, in the case of smart homes, families with infants are at a higher risk of being affected by high EMR if exposed for an extended period. This is because ample evidence indicates that infants have thinner skull thickness compared to adults, making their brains more susceptible to EMR penetration, which will probably lead to brain tumors [23], [24]. Therefore, when constructing WRNs, it is essential to guarantee the charging safety, especially for EMR exposure in critical locations where sensitive populations intend to stay a long time, like the chairs for pregnant women in the office and the head end of the cribs in the home.

Recently, considerable effort has been devoted to the EMR safety of WRNs [25]–[29]. They usually carefully select the placement positions of chargers to ensure the EMR safety, while maximizing the overall charging utility received by all devices. However, we have to point out that these traditional work ignore wave interference and instead assume that the power received by devices and critical locations is additive from different chargers.

In fact, this assumption does not align with the real-world scenarios. When two waves encounter, if the path difference between these waves is equal to $k\lambda\,(k \in N)$, constructive interference will occur, significantly increasing the power of the combined wave. Conversely, if the path difference between the two waves is equal to $(k + \frac{1}{2})\lambda\,(k \in N)$, destructive interference will greatly reduce the power of the combined wave. According to recent research [30], [31], for a WRSN deployed with 5 commercial off-the-shelf TX91501 wireless chargers [32], the power distribution is not only completely different from that in the networks assuming multiple waves are additive, but is also quite complicated. For instance, for two adjacent positions at a distance of only a few centimeters, the difference between the power at these positions actually reaches 35.23 times.

Apparently, simply applying these traditional safe charging schemes will result in serious EMR safety hazards. For example, it may cause sensitive populations to be exposed to high EMR intensity at locations deemed safe, impairing their health without awareness. Besides, neglecting wave interference may lead to some devices receiving extremely weak power due to destructive interference, drastically deteriorating the charging performance of the network. Therefore, it is essential to address the overlooked safety concerns with wave interference and develop a charging scheme benefiting from it.

In this paper, we consider a practical charging scenario containing several critical locations that are needed to guarantee EMR safety. By utilizing wave interference, we aim

Corresponding author: **Tang Liu***† (Email: liutang@sicnu.edu.cn)

to enable devices to harvest substantial power from multiple chargers while simultaneously weakening the power intensity to a sufficiently low level at critical locations. Thus, we state our Safe chArging with wave iNterferencE (SANE) problem as follows: given a fixed number of static chargers, a set of critical locations and static devices, how to design a charger placement scheme where, once the chargers are placed, both the EMR safety of critical locations and the maximization of overall charging utility for all devices are satisfied.

Generally, there are two major challenges in our problem.

The first challenge lies in building a charging model with wave interference. Not only does the charging power of a single wave attenuate nonlinearly with charging distance, but also the combined power of multiple waves fluctuates nonlinearly due to wave interference.

The second challenge is how to select the appropriate charger placement positions, to enable devices to harvest maximum power while meeting the EMR requirements of critical locations. The difficulty here arises from *(i)* the positional relationships between critical locations and devices are arbitrary; *(ii)* in the continuous search space, the positions available for charger placement are infinite.

To address the SANE problem, for the first challenge, we investigate the effects of nonlinear interference on the power distribution in the network and the EMR intensity at critical locations, and establish a charging model with wave interference. For the second challenge, we develop two discretization methods: one for approximating the power of individual waves and the other for approximating the combined power of multiple waves. These methods enable us to discretize the continuous search space into finite candidate placement subareas. From these subareas, we then identify candidate placement positions that maximize the power received by nearby devices while ensuring the EMR safety of critical locations.

The main contributions of this work are summarized below.

- To the best of our knowledge, this is the first work to consider wave interference in the field of safe charging, introducing a new research prospect in how to construct safe and efficient WRNs.
- We develop a safe charging scheme, termed SANE, to maximize the overall charging utility while ensuring the EMR safety of critical locations. Theoretical analyses are provided to prove the effectiveness of our SANE scheme.
- Extensive simulations and field experiments verify that SANE outperforms the comparison algorithms by an average of 89.65% in overall charging utility, and the EMR safety of all critical locations is ensured.

II. Preliminaries

A. Network Model

Suppose there are *N* static rechargeable devices distributed on a 2D plane Ω, which is represented by $S = \{s_1, s_2, ..., s_N\}$. If no confusion arises, we still use s_i to denote the position of the device s_i.

A given number of omnidirectional wireless chargers with the farthest charging distance D, denoted as $C = \{c_1, c_2, ..., c_M\}$, can be placed on the plane Ω to provide charging service for the devices. We still use c_k to represent the placement position of the charger c_k. When all chargers are deployed, each device s_i will be concurrently charged by a group of chargers covering it within D. We define the subset of chargers covering s_i to be C_{s_i}, which contains m_{s_i} chargers in total, and the combined power at s_i is $P_{s_i|C_{s_i}}$. We use d_{c_k,s_i} to represent the distance from charger c_k to device s_i.

Meanwhile, there are also *H* fixed critical locations on the plane Ω, denoted as $\Gamma = \{\gamma_1, \gamma_2, ..., \gamma_H\}$, needing protection from the risk of high EMR generated by the chargers. We still use γ_j to denote the position of the critical location γ_j. Similar to the devices, we assume the charger subset covering γ_j to be C_{γ_j}, which consists of m_{γ_j} chargers and imposes the combined power of $P_{\gamma_j|C_{\gamma_j}}$ on γ_j. Moreover, we use d_{c_k,γ_j} to represent the distance from charger c_k to critical location γ_j. For safe charging, an EMR safety threshold R_t is predetermined to assess the levels of EMR exposure. In Section VII, we discuss how to extend our safe charging scheme to ensure the EMR safety of critical areas.

B. Charging Model

To investigate the intricate power distribution resulting from the nonlinear wave interference, a practical charging model with wave interference needs to be built. First, we begin with the radio wave emitted from the charger c_k:

$$A(t) = A_0 \cos(2\pi f t + \phi_0), \tag{1}$$

where A_0, f, ϕ_0 are the amplitude, frequency and initial phase of the wave emitted from c_k, respectively. As the attenuation of amplitude is in a quadratic relation with distance, the wave arrived at device s_i or critical location γ_j can be accordingly expressed. Here, we take the wave arrived at s_i as an example:

$$A(t) = \frac{A_0}{\tilde{d}_{c_k,s_i}} \cos(2\pi f t + \phi_0 - \frac{2\pi}{\lambda} d_{c_k,s_i}), \tag{2}$$

where $\tilde{d}_{c_k,s_i} = \frac{d_{c_k,s_i}+\beta}{\sqrt{\alpha}}$ is the adjusted version of distance considering the attenuation in the propagation of the wave from charger c_k to device s_i. $\alpha = \frac{G_s G_r \eta}{L_P}(\frac{\lambda}{4\pi})^2$, where G_s and G_r are the antenna gains of charger and device, respectively. β is a parameter to adjust the Friis' free space equation for short distance transmission. η is the rectifier efficiency, L_p is the polarization loss, and λ is the wavelength [33].

When charger c_k charges device s_i, the wave received by s_i can be expressed with the Eq. (2). Assuming the period of the radio wave is T, the average power at s_i is:

$$\begin{aligned} p(c_k, s_i) &= \frac{1}{T}\int_{-\frac{T}{2}}^{\frac{T}{2}} \Big[A(t)\Big]^2 dt \\ &= \frac{1}{T}\int_{-\frac{T}{2}}^{\frac{T}{2}} \Big[\frac{A_0}{\tilde{d}_{c_k,s_i}} \cos(2\pi f t + \phi_0 - \frac{2\pi}{\lambda} d_{c_k,s_i})\Big]^2 dt = \frac{A_0^2}{2(\tilde{d}_{c_k,s_i})^2}. \end{aligned} \tag{3}$$

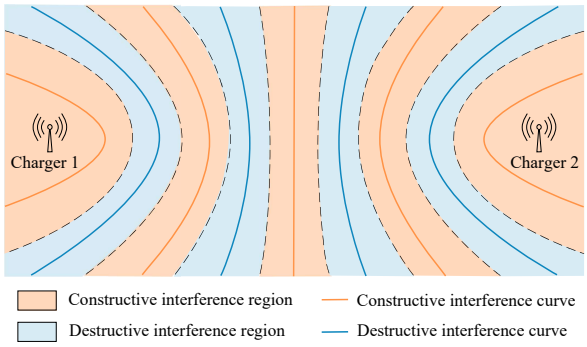

Fig. 1. Power distribution of a network with two chargers.

When m_{s_i} chargers simultaneously charge s_i, the combined wave arrived at s_i can be calculated as:

$$\begin{aligned} A_{s_i|C_{s_i}}(t) &= A_i \cos(2\pi f t - \phi) \\ &= \sum_{k=1}^{m_{s_i}} \frac{A_0}{\tilde{d}_{c_k,s_i}} \cos(2\pi f t - \frac{2\pi}{\lambda} d_{c_k,s_i}), \end{aligned} \tag{4}$$

where $A_i = \left[m_{s_i} {A_0}^2 + 2A_0^2 \sum_{k>l}^{m_{s_i}} \sum_{l=1}^{m_{s_i}} \cos(2\pi \frac{d_{c_k,s_i} - d_{c_l,s_i}}{\lambda}) \right]^{\frac{1}{2}}$ is the combined wave's amplitude and ϕ represents its phase.

Similar to the Eq. (3), the average power at s_i is:

$$\begin{aligned} P_{s_i|C_{s_i}} &= \sum_{c_k \in C_{s_i}} p(c_k, s_i) = \frac{1}{T} \int_{-\frac{T}{2}}^{\frac{T}{2}} \left[A_{s_i|C_{s_i}}(t) \right]^2 dt \\ &= \frac{A_0^2}{2} \left(\sum_{k=1}^{m_{s_i}} \frac{1}{(\tilde{d}_{c_k,s_i})^2} + \sum_{k>l}^{m_{s_i}} \sum_{l=1}^{m_{s_i}} \frac{2\cos(2\pi \frac{d_{c_k,s_i} - d_{c_l,s_i}}{\lambda})}{\tilde{d}_{c_k,s_i} \cdot \tilde{d}_{c_l,s_i}} \right). \end{aligned} \tag{5}$$

Eq. (5) reveals that the combined power received by each device is depended on the wave interference caused by the path difference among the waves from different chargers. Fig. 1 depicts the power distribution of the network with two chargers. We can see that the constructive interference regions (*i.e.*, orange regions) and destructive interference regions (*i.e.*, blue regions) appear alternately. At the center of each constructive interference region lies an orange complete constructive curve, where the path difference between any point on this curve and the two chargers is equal to $k\lambda\,(k \in N)$. For the destructive interference region, there is also a blue complete destructive curve at the center, where the path difference between any point on this curve and the two chargers is equal to $(k + \frac{1}{2})\lambda, (k \in N)$. Apparently, to achieve effective and safe charging, we should locate every device on the complete constructive curve as possible and avoid situating the critical locations in the constructive interference regions.

As for charging safety, we introduce the concept of EMR intensity to quantify the degree of EMR exposure for critical locations. Specifically, the EMR intensity of critical location γ_j can be expressed as:

$$R_{\gamma_j} = \zeta \cdot P_{\gamma_j|C_{\gamma_j}}, \tag{6}$$

where ζ is a constant value and the combined power intensity $P_{\gamma_j|C_{\gamma_j}}$ at γ_j can be calculated in the same way as devices. Depending on different environments, the EMR safety threshold R_t can be set in advance. For those critical locations with the EMR intensity below R_t, they are considered to be safe.

C. Charging Utility Model

Due to hardware constraints and practical requirements, the harvested power of devices is usually constrained with an upper bound P_{th}. Thus, we adopt a linear charging utility model for the received power, where the charging utility is first proportional to the harvested energy until it reaches a given threshold, after which it remains constant. For device s_i, the *charging utility* can be calculated as:

$$u(P_{s_i|C_{s_i}}) = \begin{cases} \frac{1}{P_{th}} \cdot P_{s_i|C_{s_i}}, & P_{s_i|C_{s_i}} < P_{th}, \\ 1, & P_{s_i|C_{s_i}} \geq P_{th}. \end{cases} \tag{7}$$

D. Problem Formulation

In this paper, our objective is to design a charger placement scheme with wave interference to construct a safe and efficient WRN. Specifically, we aim to find out a set of charger placement positions that ensures the EMR intensity at critical locations below the EMR safety threshold R_t while maximizing the overall charging utility of the network. Here, we state our Safe chArging with wave iNterferencE (SANE) problem as follows:

$$\begin{aligned} \textbf{(P1)} \quad & max \quad u(total) = \sum_{i=1}^{N} u(P_{s_i|C_{s_i}}), \\ & s.t. \quad \forall \gamma_j \in \Gamma, \quad R_{\gamma_j} \leq R_t. \end{aligned} \tag{8}$$

Theorem 1. *The SANE problem P1 is NP-hard.*

Proof: We omit the proof due to space limitations. ■

III. Area Discretization

Due to the continuous nature of the 2D plane, all positions within the network are available for placing chargers. To avoid the computational overhead arising from enumerating them, in this section, we aim to reduce the continuous search space to a limited one without performance loss. So, we first approximate the nonlinear charging power of individual waves using a piecewise constant function, and then discretize the whole network into multiple candidate placement areas.

Let $P_r(d)$ denote the power a device received from a single charger with distance d, we can give the following definition.

Definition 1. *Setting $d(0) = 0$ and $d(V) = D$, the piecewise constant function $\widetilde{P_r}(d)$ can be written as*

$$\widetilde{P_r}(d) = \begin{cases} P_r(d(1)), & d = d(0), \\ P_r(d(v)), & d(v-1) < d \leq d(v) (v = 1, ...V), \\ 0, & d > d(V). \end{cases}$$

Here, $d(1)$ to $d(V)$ represent the end points of the constant segments in order, where V denotes the number of constant segments. Additionally, V also serves as a vital parameter to control the approximation error and computational complexity.

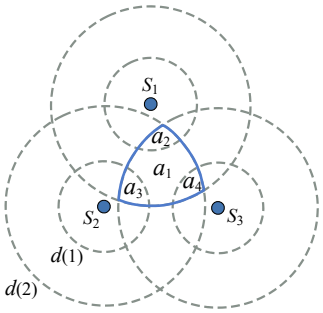

Fig. 2. An illustration of Dominant Covered Sets (DCSs) extraction.

Generally, as we increase the value of V, the approximated error reduces, but the computational complexity increases.

Moreover, we have the following theorem to describe the number of constant segments and the approximation error.

Theorem 2. *We set $d(0) = 0$, $d(V) = D$, and $d(v) = \beta((1+\epsilon_1)^{\frac{v}{2}} - 1)$, $(v = 1, ..., V-1)$. Then, we get the number of constant segments*

$$V = \lceil \frac{ln(P_r(0)/P_r(D))}{ln(1+\epsilon_1)} \rceil,$$

where ϵ_1 is a predetermined error threshold, and the approximation error satisfies

$$1 \leq \frac{P_r(d)}{\widetilde{P_r}(d)} \leq 1 + \epsilon_1, (d \leq D).$$

Based on the piecewise constant function, we can draw V concentric circles centered at each device with a radius of $d(1)$ to $d(V)$, forming V numbers of rings. Inside each discretized ring, the charging power of an individual wave is approximated as a constant. Furthermore, to maximize the overall charging utility by enabling each charger to cover as many devices as possible, we present a Dominant Covered Set extraction method based on the distribution of devices.

To start with, we have the following definitions:

Definition 2. *Dominance: Given two charger placement positions c_1 and c_2, and their corresponding covered device sets S_1 and S_2, if $S_1 = S_2$, we define that c_2 is equivalent to c_1. If $S_1 \subset S_2$, we define that c_2 dominates c_1.*

Definition 3. *Dominant Covered Set: Given a set of covered devices S_i corresponding to the charger placement position c_i, if there is no other charger placement position c_j where c_j dominates c_i, we define S_i as a Dominant Covered Set (DCS).*

Definition 4. *Candidate Placement Area: Given a DCS S_i, if there exists an area where randomly placing a charger within ensures that all devices in S_i can be covered, we define this area as a Candidate Placement Area corresponding to S_i.*

Clearly, placing chargers within the candidate placement areas of DCSs is always better than placing in the corresponding areas of its subsets. Therefore, we focus on extracting all DCSs and their corresponding candidate placement areas.

Fig. 2 gives an instance of the extraction process. In Fig. 2, there are 3 devices s_1, s_2, and s_3. Drawing concentric circles centered at each device with the radius of $d(1)$ and $d(2)$, we obtain the candidate placement area (*i.e.*, the overlapping area enclosed by the blue line) of the device set $\{s_1, s_2, s_3\}$. When a charger is placed anywhere within this area, 3 devices can be charged simultaneously. Thus, the DCS in Fig. 2 is $\{s_1, s_2, s_3\}$. Moreover, it also can be seen that the candidate placement area has been divided into 4 subareas, *i.e.*, a_1, a_2, a_3, a_4. Within each subarea, randomly placing a charger provides the same approximated power to 3 devices.

The detailed process of area discretization and dominant covering sets extraction is given in Algorithm 1.

IV. Charger Placement

After exacting all DCSs and their candidate placement areas, in this section, our objective here is to place chargers to address our SANE problem. Since the EMR safety of critical locations must be guaranteed, our basic idea is as follows: First, before placing each charger, we identify the *dangerous regions* for each critical location where chargers cannot be placed, and accordingly update each candidate placement subareas. Then, we select an updated subarea that maximizes the charging power received by surrounding devices and determine a candidate placement position within it. Finally, we select one from all candidate placement positions that can yield the maximum marginal charging utility to place a charger. This process is repeated until all chargers are placed.

A. Identifying Dangerous Regions

In this subsection, we first give the definition of *dangerous region* and then present the theorems that explain the two different shapes of the dangerous region.

Definition 5. *Dangerous Region: Given a critical location γ_i, if there exists a region where placing a charger would cause the EMR intensity at γ_i to exceed the predetermined*

Algorithm 1 Area discretization and DCSs extraction

Input: The set of devices S, the farthest charging distance D, the error threshold ϵ_1
Output: The set of candidate placement subareas A

```
for each device s_i ∈ S do
    Draw a circle centered at s_i with radius D, and discretize the circle through the piecewise constant function P̃_r(d) with the error threshold ε_1;
end for
for each area obtained after the discretization do
    Calculate the covered devices, and add the covered devices set into the set of candidate DCS;
end for
Identify all DCSs from the set of candidate DCS and add the corresponding candidate placement subareas into the set of candidate placement subareas A;
Return the set of candidate placement subareas A;
```

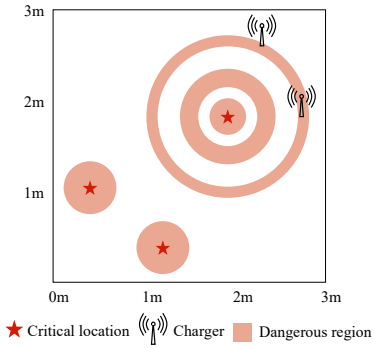

Fig. 3. A simulation of how dangerous regions are shaped with 2 chargers with the frequency of 915*MHz* placed on a 3m × 3m 2D plane.

EMR safety threshold R_t, we define this region as a dangerous region corresponding to γ_i.

When identifying the corresponding dangerous regions for each critical location, depending on whether the waves from the already placed chargers could reach the critical location, there are two shapes of dangerous regions: circle and ring.

Theorem 3. *For any critical location, when there are no chargers placed nearby, the dangerous region is a circle with the radius of $\frac{\sqrt{2}}{2}A_0\sqrt{\frac{\alpha\cdot\zeta}{R_t}}-\beta$ centered at the critical location.*

Proof: Assuming there is no charger placed around the critical location γ_1. If a charger c_1 is placed near the γ_1 with a distance d_1 to it, according to Eq. (3) and Eq. (6), the EMR intensity at γ_1 is $R_{\gamma_1}=\zeta\cdot p(c_1,\gamma_1)=\frac{\zeta\cdot {A_0}^2}{2(\frac{d_1+\beta}{\sqrt{\alpha}})^2}$.

If the c_1 causes the EMR intensity at γ_1 to equal the EMR safety threshold R_t (*i.e.*, $\frac{\zeta\cdot {A_0}^2}{2(\frac{d_1+\beta}{\sqrt{\alpha}})^2}=R_t$), the distance between c_1 and γ_1 satisfies $d_1=\frac{\sqrt{2}}{2}A_0\sqrt{\frac{\alpha\cdot\zeta}{R_t}}-\beta$. Since the EMR intensity decreases with the charging distance, as long as the charger is located within a circle centered at γ_1 with the radius of $\frac{\sqrt{2}}{2}A_0\sqrt{\frac{\alpha\cdot\zeta}{R_t}}-\beta$, the EMR intensity at γ_1 will exceed R_t.

Therefore, we can conclude that the shape of the corresponding dangerous region of γ_1 is a circle centered at γ_1 with the radius of $\frac{\sqrt{2}}{2}A_0\sqrt{\frac{\alpha\cdot\zeta}{R_t}}-\beta$. Consequently, the theorem is proven. ■

Theorem 4. *For any critical location, when there are chargers placed nearby, its corresponding dangerous region includes not only a circle centered at the critical location but also potentially several rings centered at it.*

Proof: When multiple chargers are placed near a critical location γ_1, their emitted waves interfere at γ_1. Despite the interference effects altering the amplitude of the combined wave, the frequency of the combined wave remains unchanged. Thus, based on the positions of all placed chargers, the amplitude of the combined wave can be obtained according to Eq. (4). This allows us to treat the combined wave as a wave emitted by a virtual charger c_1 located at a distance of d_1 from γ_1.

If a charger c_2 is placed near the critical location γ_1 with a distance d_2 to it, then the path difference between c_1 and c_2 to γ_1 is $\Delta d=|d_1-d_2|$. When $\Delta d=k\lambda\,(k\in N)$, complete constructive interference will occur at γ_1. For any given k, if the EMR intensity of the combined wave at γ_1 exceeds R_t with complete constructive wave interference, wherever c_2 is placed on the circle O_k centered at γ_1 with the radius of $d_1-k\lambda$ $(d_1>d_2)$ or $d_1+k\lambda$ $(d_1\le d_2)$, the EMR safety of γ_1 will be threatened.

As the placement position of c_2 deviates from circle O_k towards or away from γ_1, complete constructive interference will not occur, resulting in a gradual decrease in the EMR intensity at γ_1. When the distance between c_2 and O_k reaches a certain value, the EMR intensity at γ_1 will equal R_t. Therefore, we can conclude that the dangerous region of γ_1 is shaped as a ring centered at γ_1 which includes O_k. When k takes different values, the corresponding dangerous region of γ_1 may be multiple concentric rings centered at γ_1. Consequently, the theorem is proven. ■

Fig. 3 shows the shapes of the dangerous regions observed through simulation. We can see that there are three critical locations represented in red stars, with one of them situated in the top right corner surrounded by two nearby chargers. For each critical location, we extract its corresponding dangerous regions highlighted in brown. It can be seen that the dangerous regions of the critical location with two nearby chargers appear as a circle and two rings centered at it, meanwhile the dangerous regions of the other two critical locations, where no chargers are nearby, are all shaped in circle.

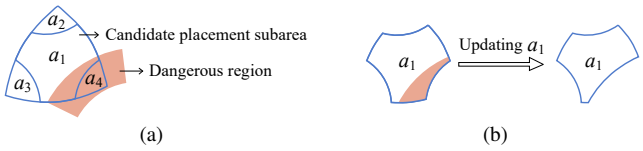

Fig. 4. An example of updating the candidate placement subareas.

B. Updating Candidate Placement Subareas

Next, in order to ensure that placing a charger can always satisfy the EMR safety of critical locations, in this subsection, we propose a method to update the candidate placement subareas based on the dangerous regions.

Based on the positional relationships between candidate placement subareas and the dangerous regions, the process of updating candidate placement subareas can be classified into three categories: *(i)* For the candidate placement subareas that do not overlap with any dangerous region, we keep them unchanged. *(ii)* For the candidate placement subareas that are partially within the dangerous regions, we reshape them by cutting out the overlapping part and keeping the remaining part as the updated version. *(iii)* For the candidate placement subareas that are entirely within the dangerous regions, we remove them from consideration.

To better understand the updating process, an example is shown in Fig. 4. In Fig. 4(a), candidate placement subareas a_2 and a_3 do not overlap with the dangerous region, so their shapes remain unchanged. As for a_1 that is partially within the

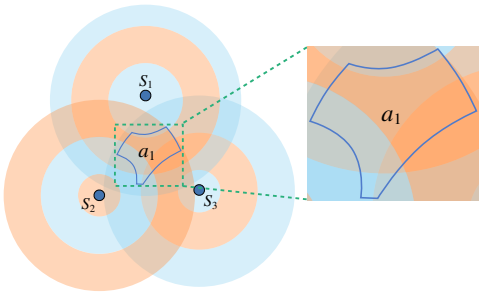

Fig. 5. An example of constructive and destructive zones within the candidate placement subarea a_1.

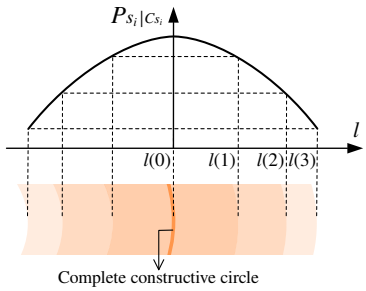

Fig. 6. Combined power approximation.

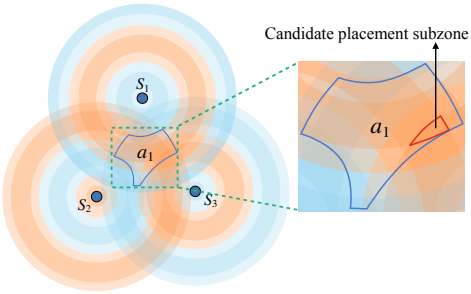

Fig. 7. An example of identifying a candidate placement position from candidate placement subarea a_1.

dangerous region, we reshape it by cutting out its overlapping part (see Fig. 4(b)). Since a_4 is entirely within the dangerous region, it is no longer a candidate placement subarea.

C. Selecting Charger Placement Position

In this subsection, our objective is to place a charger to maximize the marginal charging utility.

For each updated candidate placement subarea, placing a charger at different positions within it may result in varying interference effects on every nearby device. Obviously, to maximize the marginal charging utility, it is essential to allow the devices to receive more combined power from constructive interference. Based on the wave interference theory, we present the following definition and theorem.

Definition 6. *Constructive Zone: Given a device s_i, if there exists a zone where placing a charger can enhance the received power of s_i by constructive interference, we define this zone as a constructive zone corresponding to s_i.*

Definition 7. *Destructive Zone: Given a device s_i, if there exists a zone where placing a charger can weaken the received power of s_i by destructive interference, we define this zone as a destructive zone corresponding to s_i.*

Theorem 5. *For any device with one or more chargers already placed nearby, its corresponding constructive and destructive placement zones appear as alternating concentric zones centered at it.*

Proof: Similar to the proof of Theorem 4, when multiple chargers are placed near the device s_1, we also consider the combined wave as a wave emitted by a virtual charger c_1 located at a distance of d_1 from s_1.

If a charger c_2 is placed near the device s_1 with a distance d_2 to it, then the path difference between c_1 and c_2 to s_1 is $\Delta d = |d_1 - d_2|$. According to Eq. (5), when $\Delta d = (\frac{k}{2} + \frac{1}{4})\lambda\,(k \in N)$, the device would be located on the edge of constructive and destructive interference region. By taking different values of k, we can obtain several values of d_2 in the range of 0 to D. Setting different values of d_2 as the radius, we can draw multiple circles centered at s_1. Each pair of circles forms a concentric ring representing a constructive region or destructive region. Consequently, the theorem is proven. ■

Fig. 5 shows the orange constructive and blue destructive zones of three devices s_1, s_2, s_3. For the candidate placement subarea a_1, we can see that the intersection of these zones is quite complex. The complexity arises because these alternating constructive and destructive zones overlap each other, with each overlap having a different shape and size. This means that when a charger is placed at different positions within a_1, the power received by each device will vary. Therefore, within the continuous subarea, we need to consider the intrinsic connection between the exact charger placement position and multiple sets of nonlinear wave interference, aiming to allow multiple devices to simultaneously benefit from the high power generated by strong interference effects as much as possible.

To achieve this goal, we devise a piecewise constant function $\widetilde{P}_{s_i|C_{s_i}}(l)$ to approximate the combined power. For simplicity, we only show how to discretize the constructive zone for s_i, and the discretization of the destructive zone can be obtained similarly. According to the wave interference theory, at the center of each ring-shaped constructive zone lies a complete constructive circle, *i.e.*, when a charger is placed on it, s_i will receive the highest combined power due to complete constructive interference. As the charger's position deviates from the complete constructive circle, the effect of constructive interference decreases, resulting in a gradual reduction in the combined power received by s_i. Therefore, based on this power distribution in the constructive zone, we discretize the combined power $P_{s_i|C_{s_i}}$ by the distance l between the charger c_k and the complete constructive circle. Our piecewise constant function can be expressed as:

$$\widetilde{P}_{s_i|C_{s_i}}(l) = \begin{cases} P_{s_i|C_{s_i}}(l(1)), & l = l(0), \\ P_{s_i|C_{s_i}}(l(k)), & l(k-1) < l \le l(k) \\ & (k = 1,\ \ldots,\ K), \end{cases} \tag{9}$$

where $l(0) = 0$, $l(K) = \frac{\lambda}{4}$, and K refers to the number of subzones divided with this function. This function can also be applied when multiple chargers are placed around the device, as these placed chargers can be considered to be a virtual charger. Theoretically, we have the following lemma and theorem for this discretization:

Lemma 1. *We set $l(0) = 0$, $l(K) = \frac{\lambda}{4}$, and $l(k) = \frac{\lambda}{2\pi} \cdot \arccos\left(\frac{\left[\frac{1}{(1+\epsilon_2)^k} - 1\right](p(c_j,s_i)+p(c_k,s_i))}{2\sqrt{p(c_j,s_i)\cdot p(c_k,s_i)}}\right) + 1$. Then, we get $K = \lceil \frac{\ln(P_{s_i|C_{s_i}}(0)/P_{s_i|C_{s_i}}(\frac{\lambda}{4}))}{\ln(1+\epsilon_2)} \rceil$. For the approximated com-*

bined power $\widetilde{P}_{s_i|C_{s_i}}(l)$, the approximation error is subject to

$$1 \leq \frac{P_{s_i|C_{s_i}}(l)}{\widetilde{P}_{s_i|C_{s_i}}(l)} \leq 1+\epsilon_2, (0 \leq l \leq \frac{\lambda}{4}). \tag{10}$$

Proof: We omit the proof due to space limitations. ■

For ease of understanding, we use Fig. 6 to illustrate this combined power approximation. We can see that on each side of the complete constructive circle, the constructive zone is divided into 3 subzones. Within each subzone, regardless of the exact position of the charger, the corresponding device will receive the same approximated combined power.

Theorem 6. *Let $u(\widetilde{P}_{s_i|C_{s_i}}(l))$ represent the charging utility with the approximated combined power $\widetilde{P}_{s_i|C_{s_i}}(l)$ for s_i, the approximation error is subject to*

$$1 \leq \frac{u(P_{s_i|C_{s_i}}(l))}{u(\widetilde{P}_{s_i|C_{s_i}}(l))} \leq 1+\epsilon_2, \ (0 \leq l \leq \frac{\lambda}{4}). \tag{11}$$

Proof: We omit the proof due to space limitations. ■

Fig. 7 shows the discretized constructive and destructive zones of three devices, s_1, s_2, and s_3. After discretization, we can see that the candidate placement subarea a_1 is divided into 42 subzones. Since the combined power received by each device remains unchanged regardless of the exact position of the charger within a subzone, we only need to identify the subzone where the total combined power is maximized for the three devices, which we call the *candidate placement subzone* (*i.e.*, the subzone encircled by the red line). Any position within the candidate placement subzone can be chosen as the candidate placement position of a_1.

By applying this method, for each DCS, we can identify a candidate placement position. Then, from all these positions, we select the one that maximizes the marginal charging utility and place a charger there.

The detailed process of the charger placement algorithm is given in Algorithm 2.

Algorithm 2 Charger placement algorithm

Input: The set of devices S, the set of critical locations Γ, the set of candidate placement subareas A, the error threshold ϵ_2, and the number of chargers M
Output: The set of charger placement positions C

$C = \emptyset$
while $|C| \neq M$ **do**
  for each critical location $\gamma_i \in \Gamma$ **do**
    Extract the dangerous regions for γ_i, and accordingly update the candidate placement subareas;
  end for
  for each device $s_i \in S$ **do**
    Draw constructive and destructive zones for s_i, and discretize these zones into subzones through the piecewise constant function $\widetilde{P}_{s_i|C_{s_i}}(l)$ with the error threshold ϵ_2;
  end for
  for each updated candidate placement subarea $a_i \in A$ **do**
    Find the candidate placement subzone of a_i with the highest combined power and randomly choose a position $c_i{}'$ within this subzone, and add $c_i{}'$ into the candidate charger placement position set C';
  end for
  $c^* \leftarrow \arg\max_{c \in C' \setminus C}(u(C \cup \{c\}) - u(C))$;
  $C = C \cup \{c^*\}$;
end while
Return the set of charger placement positions C;

V. Simulations

A. Simulation Setup

We conduct simulations in a $20m \times 20m$ area with 15 critical locations and 20 devices randomly distributed. Additionally, there are 8 omnidirectional chargers to be placed, with the farthest charging distance of $D = 4m$ and the charging power of $P_0 = 3W$. The wavelength is set as $\lambda = 32.8cm$ according to the commercial off-the-shelf TX91501 wireless charger produced by Powercast [32]. For the charging model, we set $\alpha = 100$, $\beta = 40$, $P_{th} = 10mW$ [30], [31]. We also set $\zeta = 1$, $R_t = 5$ for the EMR model, and the error thresholds are set to $\epsilon_1 = 0.2$ and $\epsilon_2 = 0.2$.

To evaluate the performance of our SANE scheme, we compare it with the following four charging algorithms.

Wireless Charger Placement with EMR Safety (PESA) [28] is a safe charging algorithm that ignores wave interference. PESA maximizes the additive power received by all devices by determining the placement position of each charger while ensuring the network's EMR safety.

Wireless Charger Placement with Multiple Antennas (WANDA) [34] is an algorithm that places chargers with multiple directional antennas, without considering EMR safety. WANDA ignores wave interference and uses a greedy strategy to place each charger to maximize the additive power received by all devices. For fair comparisons, we provide WANDA with chargers equipped with omnidirectional antennas.

Randomized Safe Charger Position (RAN-S) is a safe charging algorithm developed by us that considers wave interference but places chargers randomly within the updated candidate placement subareas.

Randomized Safe Charger Position (RAN) is a charging algorithm that randomly places chargers without considering EMR safety.

B. Performance Comparisons

1) Impact of the number of devices N: Fig. 8(a) shows that on average, SANE outperforms PESA, WANDA, RAN-S, and RAN by 35.6%, 20.4%, 72.1%, and 89.5%, respectively, in terms of N. From Fig. 8(a), we can see that the overall charging utility yielded by all algorithms increases with the number of devices. Since our SANE scheme fully utilizes constructive interference to enhance the power received by the devices, it achieves the best performance.

Fig. 8(b) compares the number of unsafe critical locations where the EMR intensity exceeds the threshold R_t. We can see that our SANE scheme guarantees the EMR safety of all critical locations. It is worth noting that although PESA is a

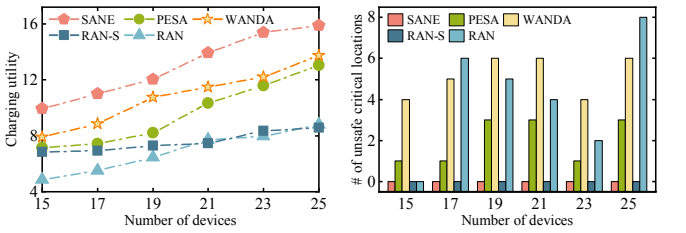

(a) Charging utility (b) Number of unsafe critical locations

Fig. 8. Performance comparisons by different numbers of devices.

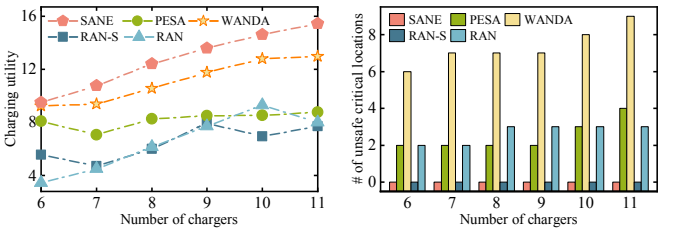

(a) Charging utility (b) Number of unsafe critical locations

Fig. 10. Performance comparisons by different numbers of chargers.

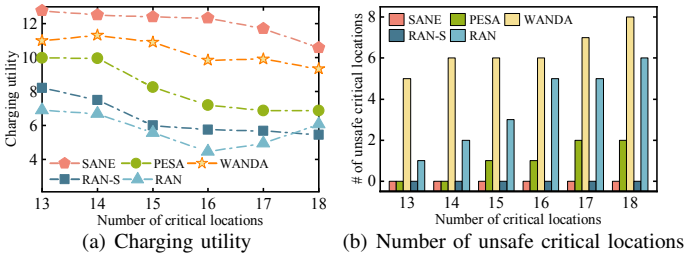

(a) Charging utility (b) Number of unsafe critical locations

Fig. 9. Performance comparisons by different numbers of critical locations.

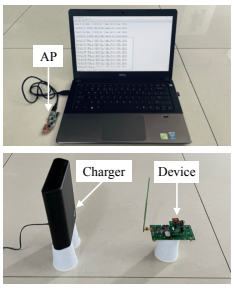

Fig. 11. Testbed.

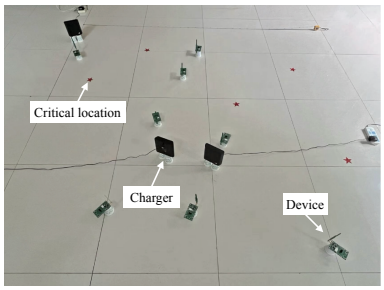

Fig. 12. Field experiment.

safe charging algorithm, it cannot guarantee the EMR safety of all critical locations due to its neglect of wave interference.

2) Impact of the number of critical locations H : Fig. 9(a) shows that on average, SANE outperforms PESA, WANDA, RAN-S, and RAN by 47.1%, 16.0%, 87.6%, and 109.0%, respectively, in terms of H. We can see that the overall charging utility of SANE decreases slightly as H increases. The reason is that a larger number of critical locations creates more dangerous regions, reducing the area available for placing chargers.

Fig. 9(b) shows that regardless of the number of critical locations in the network, our SANE scheme can ensure their EMR safety. This verifies the adaptability of the SANE scheme to WRNs with different safety requirements.

3) Impact of the number of chargers M: Fig. 10(a) shows that on average, SANE outperforms PESA, WANDA, RAN-S, and RAN by 55.0%, 14.4%, 96.4%, and 95.1%, respectively, in terms of M. It can be seen that the overall charging utility achieved by all algorithms increases with the number of chargers. Additionally, the more chargers there are, the greater the advantage of the SANE scheme.

Fig. 10(b) shows that in WRNs with different numbers of chargers, our SANE scheme ensures the EMR safety of all critical locations. This suggests that even with increased input from the power supply side, the overall safety can always be guaranteed by appropriately placing each charger.

VI. Field Experiments

A. Testbed

Fig. 11 shows our experimental testbed, which contains three wireless chargers (TX91501 power transmitters produced by Powercast [32]) and eight rechargeable devices, all placed on a $3m \times 3m$ 2D plane. An AP is connected to a laptop to report the collected data from the devices. As shown in Fig. 12, the coordinates of the eight devices are (135.5, 191.5), (235.5, 15.5), (112.5, 118.5), (65.5, 44.5), (150.5, 229.5), (135.5, 39.5), (10.5, 229.5), and (158.5, 95.5). Additionally, there are five critical locations in the 2D plane with the coordinates (34.5, 185.5), (259.5, 210.5), (277.5, 86.5), (187.5, 151.5), and (79.5, 250.5). We set $D = 1.5m$, $P_{th} = 10mW$, and $R_t = 5$. Since the TX91501 is a directional charger, when recording the experimental data, we rotate it to face the corresponding device or critical location to imitate the omnidirectional charger [9], [29], [31], [35].

B. Experimental Results

Table I demonstrates the overall charging utility and the number of unsafe critical locations for all algorithms. As for the overall charging utility, we can see that SANE outperforms PESA, WANDA, RAN-S, and RAN by 55.1%, 17.5%, 173.7%, and 112.3%, respectively. Additionally, SANE maintains zero unsafe critical locations. This verifies that SANE achieves excellent charging performance while ensuring the EMR safety of all critical locations, by utilizing constructive interference for devices and avoiding placing chargers in dangerous regions for critical locations.

Fig. 13 illustrates the charging utility of each device. It is evident that SANE enables four devices to obtain a charging utility of 1. Moreover, the charging utility variances are 0.008, 0.178, 0.107, 0.108, and 0.150, for SANE, PESA, WANDA, RAN-S, and RAN, respectively. We can see that SANE maintains the lowest variance which verifies its fairness. As shown in Fig. 14, the EMR intensity at each critical location is controlled to a low level that remains below the EMR safety threshold with SANE. These two experiments verify both the effectiveness and safety of our SANE scheme.

TABLE I
EXPERIMENTAL RESULTS FOR FIVE ALGORITHMS.

	SANE	PESA	WANDA	RAN-S	RAN
charging utility	7.753	5.000	6.597	2.833	3.652
# of unsafe critical locations	0	1	3	0	4

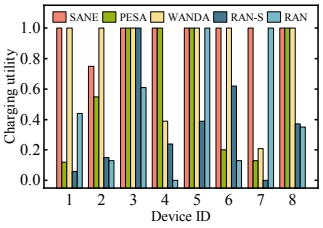

Fig. 13. Charging utility of 8 devices.

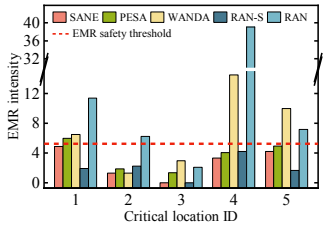

Fig. 14. EMR of 5 critical locations.

VII. DISCUSSIONS

How to achieve safe charging in practical charging scenarios with environmental objects?

When environmental objects are distributed around devices, they reflect the waves emitted by the charger, resulting in interference between these reflected waves and the direct waves. To quantify the influence of environmental objects on the EMR safety of critical locations, one way is to treat each object as a virtual charger. For any location in the network, when determining whether a charger can be placed there, we can calculate the position of the reflection point (*i.e.*, the position of the virtual charger) relative to this location. By accounting for wave attenuation [36] and half-wave loss [37] during wave reflection, we can estimate the charging power and the initial phase of the virtual charger. Thus, when applying our SANE scheme to practical scenarios with environmental objects, we can identify dangerous regions and update candidate placement subareas based on both placed chargers and virtual chargers to complete the placement of each charger, and achieve safe charging in practical charging scenarios.

How to extend the SANE scheme to WRNs with critical areas that need to ensure EMR safety?

When there are critical areas requiring EMR safety in the network, our basic idea for extending the SANE scheme is to identify the position with the highest power intensity within each critical area and then ensure the EMR intensity at these positions is below the EMR safety threshold when placing chargers. Based on this, we can identify new dangerous regions where chargers cannot be placed. After accordingly updating the candidate placement subareas, we can apply our SANE scheme to complete the placement of chargers.

VIII. RELATED WORK

Safe charging: In recent years, much effort has been devoted to achieving safe charging. [38] focused on the safe charging problem and proposed a scheduling algorithm to maximize the overall charging utility while ensuring EMR safety of the network. [39] studied how to schedule charging tasks to minimize the total charging time under the radiation constraint. In [27], the authors studied the radiation constrained fair charging problem, which aimed to maximize the minimum utility of sensors while ensuring the EMR safety. [28] concerned wireless charger placement with EMR safety and proposed a charger placement scheme to guarantee the EMR safety. In [29], the authors studied the safe charging problem with the EMR jitter phenomenon, and proposed a robust safe charging scheme based on a probabilistic model. However, all of these work ignored wave interference and assumed the charging power from different chargers to be additive, resulting in insufficient guarantee of EMR safety in the network.

Wireless charger placement. Many researchers studied the charger placement issues. [9] noticed the blocking effects of obstacles on charging waves, and proposed a charger placement scheme with obstacles. [40] utilized multi-hop wireless charging to minimize the comprehensive cost of charger placement, and devised a cost-sharing mechanism. However, wave interference is not considered in these work. In [34], the authors focused on the placement of wireless chargers with multiple directional antennas, aiming to maximize the overall charging utility by changing the positions of chargers and the orientations of antennas. In [41], the authors paid attention to the chargers with limited mobility and proposed a placement scheme for these chargers.

A few researchers have taken wave interference into account, for instance, [30] developed a charging model with wave interference and proposed an algorithm to achieve efficient concurrent charging. In [42], the authors studied how to control the power distribution of the WRSN by utilizing wave interference. Nevertheless, they do not further extend the research to the field of safe charging.

IX. CONCLUSION

In this work, we focused on the overlooked wave interference in the field of safe charging. We developed a safe charging scheme with wave interference to maximize the overall charging utility while ensuring the EMR safety of critical locations. We first designed a charging model with wave interference, and then we identified candidate placement subareas for chargers based on the EMR safety requirements of critical locations. Subsequently, we determined a candidate placement position within each subarea by leveraging the nature of wave interference. Extensive experimental results demonstrated that our proposed SANE algorithm significantly outperforms the comparison algorithms in overall charging utility while ensuring the EMR safety of all critical locations.

ACKNOWLEDMENT

This work is partially supported by the National Natural Science Foundation of China (62072320, 62002250, 62162057), the Natural Science Foundation of Sichuan Province (2022NSFSC0569, 2022NSFSC0929, 2021JDRC0004), the Humanities and Social Science Fund of Ministry of Education of China (23YJA630114), and the Key Laboratory of Data Protection and Intelligent Management of the Ministry of Education, China (SCUSAKFKT202402Y).

REFERENCES

[1] A. Kurs, A. Karalis, R. Moffatt, J. D. Joannopoulos, P. Fisher, and M. Soljacic, "Wireless power transfer via strongly coupled magnetic resonances," *Science*, vol. 317, no. 5834, pp. 83–86, 2007.

[2] M. Ren, H. Dai, T. Liu, X. Deng, W. Dou, Y. Yang, and G. Chen, "Understanding wireless charger networks: Concepts, current research, and future directions," *IEEE Communications Surveys & Tutorials*, 2024, early access.

[3] W. Yang, C. Lin, H. Dai, P. Wang, J. Ren, L. Wang, G. Wu, and Q. Zhang, "Robust wireless rechargeable sensor networks," *IEEE/ACM Transactions on Networking*, vol. 31, no. 3, pp. 949–964, 2023.

[4] J. Liu, J. Peng, W. Xu, W. Liang, T. Liu, X. Peng, Z. Xu, Z. Li, and X. Jia, "Maximizing sensor lifetime via multi-node partial-charging on sensors," *IEEE Transactions on Mobile Computing*, vol. 22, no. 11, pp. 6571–6584, 2023.

[5] W. Huang, Z. Zhao, Z. Wang, G. Min, Z. Chang, L. Fu, and H. Duan, "Adaptive mobile recharge scheduling with rapid data sharing in wireless rechargeable networks," *IEEE Transactions on Mobile Computing*, vol. 23, no. 4, pp. 3092–3105, 2024.

[6] S. He, K. Hu, S. Li, L. Fu, C. Gu, and J. Chen, "A robust RF-based wireless charging system for dockless bike-sharing," *IEEE Transactions on Mobile Computing*, vol. 23, no. 3, pp. 2395–2406, 2024.

[7] T. Liu, M. Ren, D. Wu, J. Xue, J. Li, S. Mao, and W. Xu, "Utilizing the neglected back lobe for directional charging scheduling," *IEEE Transactions on Mobile Computing*, vol. 23, no. 6, pp. 7408–7421, 2024.

[8] J. Xue, D. Wu, J. Peng, W. Xu, and T. Liu, "Charger placement with wave interference," *IEEE Transactions on Mobile Computing*, vol. 24, no. 1, pp. 261–275, 2025.

[9] W. You, M. Ren, Y. Ma, D. Wu, J. Yang, X. Liu, and T. Liu, "Practical charger placement scheme for wireless rechargeable sensor networks with obstacles," *ACM Transactions on Sensor Networks*, vol. 20, no. 1, pp. 1–23, 2024.

[10] S. Wu, H. Dai, L. Liu, L. Xu, F. Xiao, and J. Xu, "Cooperative scheduling for directional wireless charging with spatial occupation," *IEEE Transactions on Mobile Computing*, vol. 23, no. 1, pp. 286–301, 2024.

[11] W. Zhou, H. Zhou, X. Cui, X. Wang, X. Wang, and Z. Liu, "Roland: Robust in-band parallel communication for magnetic MIMO wireless power transfer system," in *IEEE INFOCOM*, 2023, pp. 1–10.

[12] (2024) Wireless chargers for medical devices: Resonant link. [Online]. Available: https://www.resonant-link.com/solutions/implantable-medical-devices

[13] Z. Yu, F. T. Alrashdan, W. Wang, M. Parker, X. Chen, F. Y. Chen, J. Woods, Z. Chen, J. T. Robinson, and K. Yang, "Magnetoelectric backscatter communication for millimeter–sized wireless biomedical implants," in *ACM MobiCom*, 2022, pp. 432–445.

[14] X. Fan, L. Shangguan, R. Howard, Y. Zhang, Y. Peng, J. Xiong, Y. Ma, and X.-Y. Li, "Towards flexible wireless charging for medical implants using distributed antenna system," in *ACM MobiCom*, 2020, pp. 1–15.

[15] (2024) Wireless charging for smart city infrastructure. [Online]. Available: https://electreon.com/what-we-do/municipalities

[16] (2024) Zens smart office. [Online]. Available: https://zens.tech/wireless-charging-for-business/zens-smart-office/

[17] P. Zhou, C. Wang, and Y. Yang, "Design and optimization of electric autonomous vehicles with renewable energy source for smart cities," in *IEEE INFOCOM*, 2020, pp. 1399–1408.

[18] (2024) RF exposure lab. [Online]. Available: https://www.rfexposurelab.com/wireless-charging-systems-for-medical-devices/

[19] (2024) The integration of wireless technology in home appliances. [Online]. Available: https://utilitiesone.com/the-integration-of-wireless-technology-in-home-appliances

[20] T. Wu, P. Yang, and H. Dai, "Charging on the move: Scheduling static chargers with tunable power for mobile devices," in *IEEE/ACM IWQOS*, 2021, pp. 1–10.

[21] M. Olteanu, C. Marincas, and D. Rafiroiu, "Dangerous temperature increase from EM radiation around metallic implants," *Acta Electrotehnica*, vol. 53, no. 2, pp. 175–180, 2012.

[22] M. P. Ntzouni, A. Skouroliakou, N. Kostomitsopoulos, and L. H. Margaritis, "Transient and cumulative memory impairments induced by GSM 1.8 GHz cell phone signal in a mouse model," *Electromagn. Biol. Med.*, vol. 32, no. 1, pp. 95–120, 2013.

[23] M. Havas, J. Marrongelle, B. Pollner, E. Kelley, C. Rees, L. Tully *et al.*, "Provocation study using heart rate variability shows microwave radiation from 2.4 GHz cordless phone affects autonomic nervous system," *Eur. J. Oncol. Library*, vol. 5, no. 1, pp. 273–300, 2010.

[24] O. P. Gandhi, L. L. Morgan, A. A. De Salles, Y.-Y. Han, R. B. Herberman, and D. L. Davis, "Exposure limits: the underestimation of absorbed cell phone radiation, especially in children," *Electromagnetic biology and medicine*, vol. 31, no. 1, pp. 34–51, 2012.

[25] R. Dai, Y. Zhao, G. Chen, W. Dou, C. Tian, X. Wu, and T. He, "Robustly safe charging for wireless power transfer," in *IEEE INFOCOM*, 2018, pp. 378–386.

[26] H. Dai, Y. Liu, G. Chen, X. Wu, T. He, A. X. Liu, and Y. Zhao, "SCAPE: Safe charging with adjustable power," *IEEE/ACM Transactions on Networking*, vol. 26, no. 1, pp. 520–533, 2018.

[27] L. Li, H. Dai, G. Chen, J. Zheng, W. Dou, and X. Wu, "Radiation constrained fair charging for wireless power transfer," *ACM Transactions on Sensor Networks*, vol. 15, no. 2, pp. 1–33, 2019.

[28] H. Dai, Y. Liu, N. Yu, C. Wu, G. Chen, T. He, and A. X. Liu, "Radiation constrained wireless charger placement," *IEEE/ACM Transactions on Networking*, vol. 29, no. 1, pp. 48–64, 2021.

[29] H. Dai, Y. Xu, G. Chen, W. Dou, C. Tian, X. Wu, and T. He, "ROSE: Robustly safe charging for wireless power transfer," *IEEE Transactions on Mobile Computing*, vol. 21, no. 6, pp. 2180–2197, 2022.

[30] Y. Ma, D. Wu, M. Ren, J. Peng, J. Yang, and T. Liu, "Concurrent charging with wave interference," in *IEEE INFOCOM*, 2023, pp. 1–10.

[31] T. Liu, Y. Ma, M. Ren, J. Yang, J. Peng, J. Yang, and D. Wu, "Concurrent charging with wave interference for multiple chargers," *IEEE/ACM Transactions on Networking*, vol. 32, no. 3, pp. 2525–2538, 2024.

[32] Powercast. [Online]. Available: https://www.powercastco.com/

[33] S. He, J. Chen, F. Jiang, D. K. Yau, G. Xing, and Y. Sun, "Energy provisioning in wireless rechargeable sensor networks," *IEEE Transactions on Mobile Computing*, vol. 12, no. 10, pp. 1931–1942, 2013.

[34] H. Dai, Y. Zhang, W. Wang, R. Gu, Y. Qu, C. Lin, L. Xu, J. Zheng, W. Dou, and G. Chen, "Placing wireless chargers with multiple antennas," *IEEE Transactions on Mobile Computing*, vol. 23, no. 6, pp. 7517–7536, 2024.

[35] C. Lin, W. Yang, H. Dai, M. S. Obaidat, L. Wang, G. Wu, and Q. Zhang, "Maximizing charging utility with fresnel diffraction model," *IEEE Transactions on Mobile Computing*, 2024, early access.

[36] T. Koppel, A. Shishkin, H. Haldre, N. Toropovs, I. Vilcane, and P. Tint, "Reflection and transmission properties of common construction materials at 2.4 GHz frequency," *Energy Procedia*, vol. 113, pp. 158–165, 2017.

[37] Z. Zhang, K. Mu, L. Zhang, and C. Zhang, "Measuring the phase shift and polarity reversal of terahertz pulse due to half-wave loss," in *SPIE The International Society for Optical Engineering*, 2011, pp. 466–471.

[38] H. Dai, Y. Liu, G. Chen, X. Wu, T. He, A. X. Liu, and H. Ma, "Safe charging for wireless power transfer," *IEEE/ACM Transactions on Networking*, vol. 25, no. 6, pp. 3531–3544, 2017.

[39] H. Dai, H. Ma, A. X. Liu, and G. Chen, "Radiation constrained scheduling of wireless charging tasks," *IEEE/ACM Transactions on Networking*, vol. 26, no. 1, pp. 314–327, 2018.

[40] S. Wu, H. Dai, L. Xu, L. Liu, F. Xiao, and J. Xu, "Comprehensive cost optimization for charger deployment in multi-hop wireless charging," *IEEE Transactions on Mobile Computing*, vol. 22, no. 8, pp. 4563–4577, 2023.

[41] H. Dai, X. Wang, X. Lin, R. Gu, S. Shi, Y. Liu, W. Dou, and G. Chen, "Placing wireless chargers with limited mobility," *IEEE Transactions on Mobile Computing*, vol. 22, no. 6, p. 3589–3603, 2023.

[42] Y. Ma, D. Wu, J. Gao, W. Sun, J. Yang, and T. Liu, "Dynamic power distribution controlling for directional chargers," in *IEEE INFOCOM*, 2024, pp. 1–10.